Thin Films

DOI: 10.1002/ange.200900461

On-Wafer Crystallization of Ultralow-κ Pure Silica Zeolite Films**

Yan Liu, Christopher M. Lew, Minwei Sun, Rui Cai, Junlan Wang, Grant Kloster, Boyan Boyanov, and Yushan Yan**

In memory of Yan Liu (1980–2009)

The continuous downscaling of microprocessors demands the timely development of ultra-low-dielectric-constant (κ) materials to reduce parasitic capacitance, enable faster switching speeds, and lower power dissipation.[1–3] The stringent requirements for the ultra-low-κ films by 2012 include not only a low κ value of 1.8 to 2.1,[1] but also high thermal conductivity, high mechanical strength, low surface roughness, high degree of hydrophobicity, and uniform pore size distribution.[4,5] While the semiconductor industry has developed suitable alternative films with the κ values between 2.5 and 2.9, viable materials with a κ value below 2.1 have not been identified.[1,6]

Pure silica zeolite (PSZ) films having MFI- and MEL-type structures are promising ultra-low-κ candidates.[7–16] Owing to their crystallinity, PSZs, such as sol-gel silica and mesoporous silica, possess stronger mechanical strength, higher heat conductivity, and higher thermal stability than alternative amorphous low-κ materials with similar porosity and κ values.[8,15–18] Two film deposition techniques have been developed: in situ crystallization and spin-on of a hydrothermally synthesized zeolite nanoparticle suspension.[10,11,16,17,19] The spin-on process is considered more attractive for commercial applications than in situ crystallization owing to the higher throughput and ability to tune film thickness with established techniques, such as spin speed and viscosity adjustments. One major challenge for the spin-on process is that it requires a zeolite nanoparticle suspension with small particle size and high zeolite yield simultaneously because large particles lead to rough surfaces and striations, and low zeolite yields generate spin-on films with low mechanical strength, low hydrophobicity, and relatively high κ values.[15–18] To achieve the necessary zeolite yield (> 60 wt %), the conventional one-stage hydrothermal synthesis method produces crystals of micrometer size, which are too large for spin-coating. Recently a two-stage synthesis technique was developed to achieve small zeolite particles with high yield by decoupling nucleation and crystal growth.[16] Specifically, the synthesis solution was first heated to and maintained at 80 °C for several days for nucleation without crystal growth, and then the temperature was increased abruptly to 114 °C and kept at that temperature for several hours for the formation of small crystals. This two-stage hydrothermal synthesis produced PSZ particles (MEL-type structure) of about 80 nm diameter with a crystal yield of 60 wt %.[16] Further improvement was obtained by an evaporation-assisted two-stage synthesis method, where an evaporation process was added between the nucleation and crystal growth to increase secondary nucleation. The nanoparticle suspension synthesized with this method showed a bimodal particle size distribution at 60 nm and 14 nm at a crystal yield of 60 wt %.[20] The spin-on films from both two-stage and the evaporation-assisted two-stage synthesis suspensions possess κ values as low as 1.9 and have good mechanical strength. However, in both cases, the crystal sizes of the suspension are still of concern and may lead to large mesopores, rough film surfaces, and difficulty in accommodating small chip features (< 30 nm). Thus, it is highly desirable to develop a simple film deposition method that is not constrained by the conflicting requirements of small crystal size and high yield.

In the aforementioned PSZ (MEL-type structure) nanoparticle suspension by the two-stage synthesis, about 60 wt % of the silica is clearly in the form of zeolite crystals (80 nm diameter). The rest of the silica was assumed to be amorphous. However, we demonstrate herein that this assumption is incorrect. High-resolution transmission electron microscopy (HRTEM, Figure 1) images were obtained from the MEL-type films (H-MEL) deposited using the two-stage hydrothermally synthesized nanoparticle suspension. Both long-range lattice fringes of about 60–80 nm (Figure 1a) and short-range lattice fringes of about 10 nm were observed (Figure 1b). It is believed that the 60 nm lattice fringes are from the large discrete MEL-type crystals that account for 60 wt % of the silica in the suspension, whereas the 10 nm lattice fringes are from the crystallization of the rest of the silica, which is 40 wt % of the total silica. This observation suggests that crystallization had occurred for the 40 wt % of the silica during the annealing of the spin-on films. To verify this hypothesis, the nanocrystals were centrifuged from the two-stage-synthesized nanoparticle suspension. The leftover

[*] Prof. J. Wang
Department of Mechanical Engineering
University of Washington, Seattle, WA 98195 (USA)
E-mail: junlan@u.washington.edu
Y. Liu, Dr. C. M. Lew, Dr. M. Sun, Dr. R. Cai, Prof. Y. Yan
Department of Chemical and Environmental Engineering
University of California, Riverside, CA 92521 (USA)
Fax: (+1) 951-827-5696
E-mail: yushan.yan@ucr.edu
Dr. G. Kloster, Dr. B. Boyanov
Intel Corporation, Hillsboro, OR (USA)

[**] κ is the relative dielectric constant of the material. We thank Steven McDaniel at CFAMM of UCR for assistance in obtaining TEM images. We acknowledge financial support from the NSF (CTS-0404376) and the Semiconductor Research Corporation through collaboration with Intel Corporation.

Supporting information for this article is available on the WWW under http://dx.doi.org/10.1002/anie.200900322.

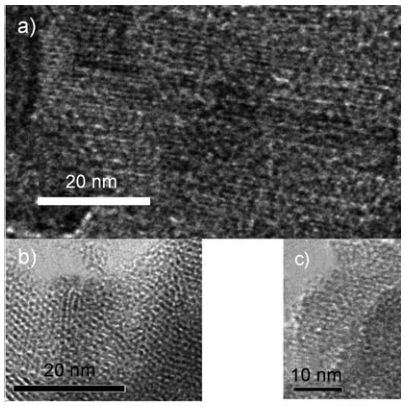

Figure 1. HRTEM images of a) 60–80 nm long-range lattice fringes from H-MEL films, b) 10 nm short-range lattice fringes from H-MEL films, and c) 10 nm short-range lattice fringes from L-MEL films.

solution was examined by dynamic light scattering (DLS); however, no particles were detected. The films spin-coated with the leftover solutions were later annealed at 400 °C. HRTEM images of the spin-on films before annealing showed no lattice fringes. However, short-range lattice fringes similar to those observed in H-MEL films appeared after annealing (Figure 1 c).

These annealed films from the leftover solutions are termed as L-MEL films and the films before the annealing termed as L-MEL precursor. The L-MEL precursor possesses MEL nuclei and the conversion from nucleated precursor into crystalline films occurs during the annealing process, which is referred herein as on-wafer crystallization. The most significant advantage of the on-wafer crystallization process is its ability to produce a zeolite spin-on film from a solution that has no particles, and thus avoid the trade-off between particle size and yield. Although the L-MEL films showed crystallinity, their preparation process is inefficient and potentially expensive because it uses a two-stage synthesis of a nanoparticle suspension that requires the use of a centrifuge and disposal of the nanocrystals (60 wt % of the total silica). A much simpler pathway is to take the nucleated solution from the first-stage of the nucleation process (forgoing the second-stage) and use it directly for spin coating followed by crystallization on the wafer. This allows for the utilization of 100 wt % of the silica and eliminates the second-stage (hydrothermal synthesis and centrifugation processes). The nucleated solution is referred as A-MEL precursor (A for aged) and the films from A-MEL precursor after annealing are referred as A-MEL films.

X-ray diffraction (XRD, Figure 2 a) and Fourier transform infrared spectroscopy (FTIR, Figure 2 b) show similar changes during annealing of L-MEL and A-MEL precursor nanoparticles. The XRD patterns of L-MEL and A-MEL show the characteristic peaks of the MEL-type structure (but relatively broad due to small crystal size). The A-MEL precursor film is clearly amorphous. FTIR spectra show that all the silicate bands (1100–1020 (vs), 800–700 (mw), and 480–440 cm^{-1} (s)[21]) are stronger after annealing owing to better cross-linking and ordering of the silica. According to the Flanigen-Khatami-Szymanski correlation, band B (480–

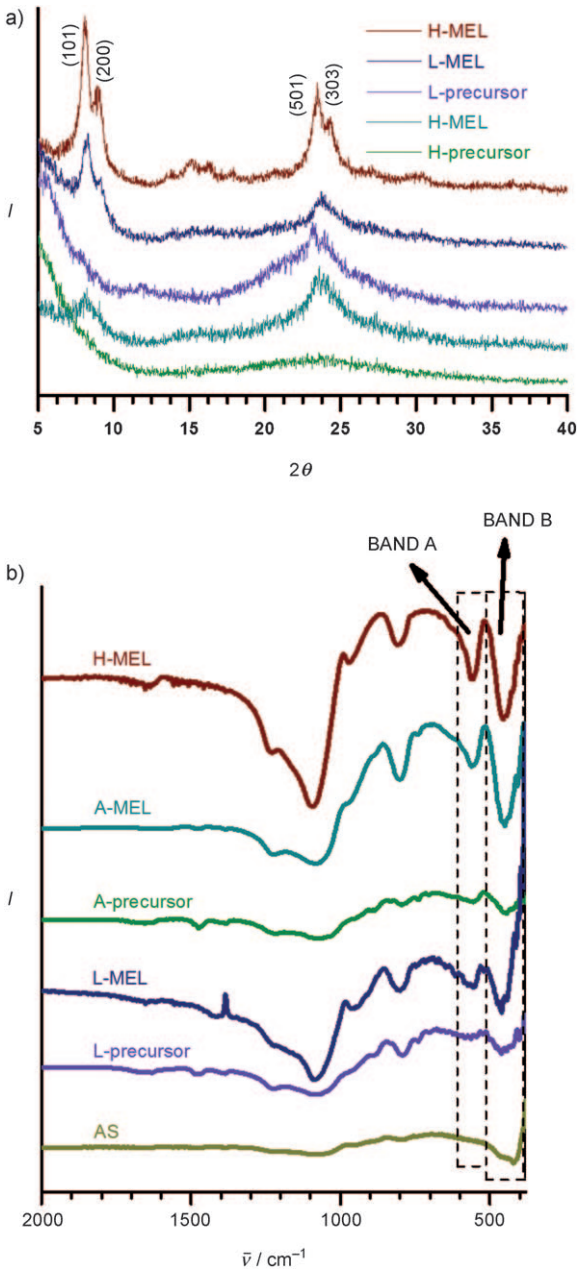

Figure 2. a) XRD patterns and b) FTIR spectra of different silicas.

440 cm^{-1}) is observed in all silicas, including quartz and amorphous silica,[21,22] whereas band A (650–550 cm^{-1}) has been assigned to the zeolite MEL framework. Therefore, the peak area ratio of bands A and B of silica is indicative of its similarity to the MEL-type structure. The ratio of the area of the two bands are listed in Table 1. For comparison, the data for an amorphous silica (AS) is also included. The A/B ratios for both L-MEL precursor and A-MEL precursor increase after annealing, indicating an increase in crystallinity. However, the A/B ratio for both films is lower than that of H-MEL owing to the smaller crystal size and unavoidable defects. Note that the amorphous silica (AS) after annealing resulted in a very low value for the A/B ratio. The XRD and FT-IR results indicate that the L-MEL and A-MEL precursors

Table 1: Ratio of the area of band A to band B from FTIR spectra of different silica.

Silica type	A/B
H-MEL	0.718
A-MEL	0.546
A-precursor	0.234
L-MEL	0.446
L-precursor	0.215
AS	0.005

possess nuclei which can undergo on-wafer crystallization during annealing to grow into a MEL-type structure and thereafter may possess all the desirable film features for low-κ applications.

For porous low-κ films, the pore sizes are required to be small and uniform to reduce the need for pore sealing, increase the chemical stability of the material, and enable the deposition of continuous copper barriers with existing techniques.[23] Spin-on zeolite films have a bimodal pore size distribution. The intracrystal micropores of less than 1 nm diameter are not considered a problem during semiconductor processing. However, the packing of the zeolite particles (ca. 80 nm) in the H-MEL films could result in large mesopores[24] that create significant concern regarding material integration and pose a potential reliability problem. The mesopores in both the H-MEL and A-MEL films were measured from the toluene adsorption/desorption isotherms. For the A-MEL films no hysteresis was observed, indicating uniform mesopores with diameters of less than 6 nm (Figure 3).[25] In contrast, the H-MEL films show significant hysteresis, confirming the presence of large and non-uniform pores connected by narrow channels (Figure 3). A-MEL precursor grows into nanoparticles with small and uniform size during on-wafer crystallization. Therefore, the packing-induced mesopores are uniform and small with an average size of 3.2 nm. These smaller mesopores may allow pore sealing to be used which avoids electrical breakdown owing to the diffusion of copper or other conductive species.[24] For the H-MEL films consisting of large crystals and small L-MEL particles (as shown in Figure 3 inset), the mesopore sizes are centered around 4.7 nm with a broad distribution. These large mesopores could lead not only to electrical breakdown, but also poor mechanical properties of the films. Using on-wafer crystallization, the packing-induced mesopores in the A-MEL films are smaller and more uniform than those in the H-MEL films.

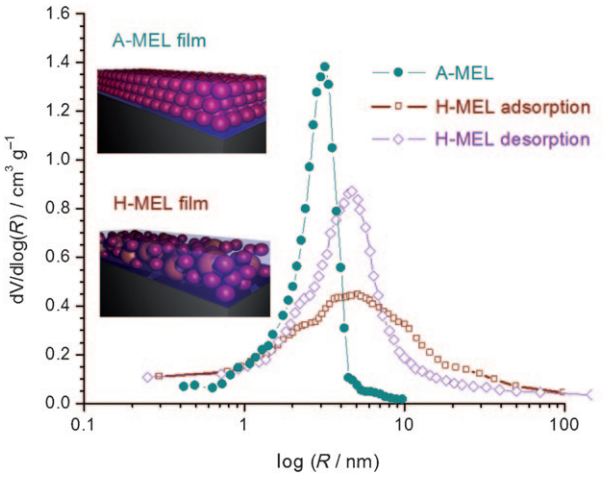

Figure 3. Mesopore radius (R) distribution in A-MEL and H-MEL films calculated from toluene adsorption and desorption isotherms obtained by ellipsometric porosimetry. Insets: schematics of particle packing.

In addition to uniform and small mesopores, other important properties for low-κ materials include a low κ value, high elastic modulus, high hardness, and low surface roughness. The κ values for A-MEL and H-MEL films are similar, but the modulus and hardness of the A-MEL films are two to three times higher, and the surface roughness is better controlled (Table 2). The low-κ materials need to be mechanically strong because they have to withstand significant stress and survive chemical mechanical polishing as well as chip packaging.[18] As the cracking velocity is inversely proportional to the film elastic modulus, the elastic modulus is often used as an indicator of the capability for the low-κ films to survive the stress induced during chip processing and packaging.[23] A threshold value of 6 GPa has been proposed as the minimum requirement;[17] however, higher values are desirable for better performance. As the A-MEL films have much smaller and more uniform mesopores, the elastic modulus (E) of the A-MEL film is more than double that of the H-MEL film, and its hardness (H) is around 3.5 times that of the H-MEL film. The E value of the A-MEL films is the highest elastic modulus ever reported for dielectric films with $\kappa < 2$. The optical microscopy images show that the H-MEL film is striated (Figure 4a). In contrast, the A-MEL film is striation-free (Figure 4b). The surface roughness (R_{rms}) value of the A-MEL films is only about 25% of that of the H-MEL films (Figure 4c and d, Table 2), further indicating the smoothness and uniformity of the A-MEL films.

Table 2: Comparison of the film properties of ultra low-κ A-MEL and H-MEL dielectric films.

Film	κ value	Elastic modulus E [GPa]	Hardness H [GPa]	Surface roughness R_{rms} [nm]
H-MEL	1.9 ± 0.1	7.89 ± 0.44	0.43 ± 0.02	11.2 ± 0.8
A-MEL	1.8 ± 0.2	16.78 ± 0.73	1.52 ± 0.07	2.9 ± 0.1

In conclusion, we have developed a simple and efficient on-wafer crystallization method to deposit zeolite films for ultra-low-κ application. Spin-on of the clear precursor solution avoids the trade-off between crystal size and yield of the PSZs. As a result, the A-MEL films are superior to our previously developed H-MEL films in terms of the required properties for ultra-low-κ dielectrics, such as the κ value, elastic modulus, hardness, film striation, surface roughness, mesopore size, and size distribution. The on-wafer crystallization process is a significant improvement over the previously developed spin-on process, which involves a second-stage nanoparticle suspension synthesis under autogenous pressure in a sealed reactor. The on-wafer crystallization process eliminates the second-stage hydrothermal syn-

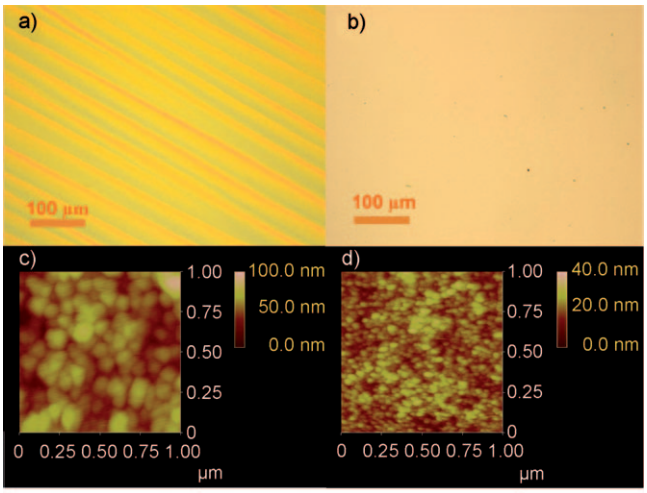

Figure 4. Optical microscopy images of a) H-MEL films and b) A-MEL films. AFM images of c) H-MEL films and d) A-MEL films.

thesis and thus no pressurized vessels are required, indicating lower cost and a more manufacturing-friendly process. Moreover, the ambient pressure nucleation and on-wafer crystallization procedure allow for fine tuning the film properties for different applications. Our ongoing work is focused on the investigation on the mechanisms of the structural transformation during the on-wafer crystallization. This 'solid-phase' transformation process may provide unique insights into the mechanistic principles of the PSZ MEL crystallization.

Experimental Section

H-MEL suspension was synthesized as follows: Tetraethyl orthosilicate (TEOS, 98%, Aldrich; 30 g), tetrabutylammonium hydroxide (TBAOH, 40%, Sachem; 27.46 g), and double deionized (DDI) water (14 g) were mixed at room temperature for one day. The corresponding molar composition was 1 TEOS/0.3 TBAOH/12 H_2O. The obtained solution was heated at 80 °C with stirring in an oil bath for 2 days and subsequently at 114 °C in a teflon-lined autoclave for 1 day. The L-MEL precursor was the leftover solution after centrifugation of the H-MEL suspension for 3 h at 20000 rpm using a Beckman J2-HS. The A-MEL precursor was synthesized with the same synthesis composition as the one used for the H-MEL suspension but at 80 °C for 13 days. Amorphous silica (AS) was obtained by stirring the mixture of 1 TEOS (10 g, 98%)/0.1 TBAOH (2.22 g, 40%)/3 ethanol (6.63 g)/32.58 DDI water (28.17 g) for 4 h at room temperature. The H-MEL suspension, L-MEL precursor, and A-MEL precursor were diluted in pentanol and spun onto the silicon substrates on a Laurell spin coater (WS-400A-6NPP/LITE) at 3000 rpm and room temperature. The obtained films were heated in air for 8 h at 80 °C and subsequently annealed in air at 400 °C for 2 h to grow the precursor films into MEL-type films as well as to remove the structure-directing agent. All the heating rates were 1 K min^{-1} and the thermal treatments were carried out at ambient pressure. For XRD and FTIR characterizations, the L- and A- precursors and H-MEL suspension were dehydrated into powder at room temperature in a vacuum, and then heated in air with the same heating program used for annealing the films.

Received: January 23, 2009
Published online: May 22, 2009

Keywords: inorganic thin films · on-wafer crystallization · silica · structure–property relationships · zeolites

[1] International Technology Roadmap for Semiconductors (2006 Edition; URL: http://www.itrs.net/).
[2] M. Creatore, W. M. M. Kessels, Y. Barrell, J. Benedikt, M. C. M. van de Sanden, *Mater. Sci. Semicond. Process.* **2004**, *7*, 283.
[3] P. S. Peercy, *Nature* **2000**, *406*, 1023.
[4] M. Morgen, E. T. Ryan, J. H. Zhao, C. Hu, T. H. Cho, P. S. Ho, *Annu. Rev. Mater. Sci.* **2000**, *30*, 645.
[5] K. Maex, M. R. Baklanov, D. Shamiryan, F. Iacopi, S. H. Brongersma, Z. S. Yanovitskaya, *J. Appl. Phys.* **2003**, *93*, 8793.
[6] R. Q. Su, T. E. Muller, J. Prochazka, J. A. Lercher, *Adv. Mater.* **2002**, *14*, 1369.
[7] S. Li, Z. J. Li, Y. S. Yan, *Adv. Mater.* **2003**, *15*, 1528.
[8] M. E. Davis, *Nature* **2002**, *417*, 813.
[9] S. Eslava, F. Iacopi, M. R. Baklanov, C. E. A. Kirschhock, K. Maex, J. A. Martens, *J. Am. Chem. Soc.* **2007**, *129*, 9288.
[10] Z. B. Wang, H. T. Wang, A. Mitra, L. M. Huang, Y. S. Yan, *Adv. Mater.* **2001**, *13*, 746.
[11] Z. B. Wang, A. P. Mitra, H. T. Wang, L. M. Huang, Y. S. Yan, *Adv. Mater.* **2001**, *13*, 1463.
[12] S. Li, J. N. Sun, Z. J. Li, H. G. Peng, D. Gidley, E. T. Ryan, Y. S. Yan, *J. Phys. Chem. B* **2004**, *108*, 11689.
[13] S. Li, Z. J. Li, D. Medina, C. Lew, Y. S. Yan, *Chem. Mater.* **2005**, *17*, 1851.
[14] C. M. Lew, Z. J. Li, S. Li, S. J. Hwang, Y. Liu, D. I. Medina, M. W. Sun, J. L. Wang, M. E. Davis, Y. S. Yan, *Adv. Funct. Mater.* **2008**, *18*, 3454.
[15] Z. J. Li, S. Li, H. M. Luo, Y. S. Yan, *Adv. Funct. Mater.* **2004**, *14*, 1019.
[16] Z. J. Li, C. M. Lew, S. Li, D. I. Medina, Y. S. Yan, *J. Phys. Chem. B* **2005**, *109*, 8652.
[17] Z. J. Li, M. C. Johnson, M. W. Sun, E. T. Ryan, D. J. Earl, W. Maichen, J. I. Martin, S. Li, C. M. Lew, J. Wang, M. W. Deem, M. E. Davis, Y. S. Yan, *Angew. Chem.* **2006**, *118*, 6477; *Angew. Chem. Int. Ed.* **2006**, *45*, 6329.
[18] M. Johnson, Z. J. Li, J. L. Wang, Y. S. Yan, *Thin Solid Films* **2007**, *515*, 3164.
[19] W. Chaikittisilp, M. E. Davis, T. Okubo, *Chem. Mater.* **2007**, *19*, 4120.
[20] Y. Liu, M. W. Sun, C. M. Lew, J. L. Wang, Y. S. Yan, *Adv. Funct. Mater.* **2008**, *18*, 1732.
[21] S. L. Burkett, M. E. Davis, *J. Phys. Chem.* **1994**, *98*, 4647.
[22] G. Coudurier, C. Naccache, J. C. Vedrine, *J. Chem. Soc. Chem. Commun.* **1982**, 1413.
[23] G. Dubois, R. D. Miller, W. Volksen in *Dielectric Films for Advanced Miroelectronics* (Eds.: M. R. Baklanov, M. Green, K. Maex), Wiley, Chichester, **2007**.
[24] S. Eslava, M. R. Baklanov, A. V. Neimak, F. Iacopi, C. E. A. Kirschhock, K. Maex, J. A. Martens, *Adv. Mater.* **2008**, *20*, 3110.
[25] P. I. Ravikovitch, A. V. Neimark, *Langmuir* **2002**, *18*, 9830.